2021

HUMAN ORGANIC ANION TRANSPORTERS 1 AND 3: STRUCTURAL ELEMENTS IMPACTING TRANSPORTER-SUBSTRATE BINDING INTERACTIONS

Julie Nguyen
Virginia Commonwealth University

HUMAN ORGANIC ANION TRANSPORTERS 1 AND 3: STRUCTURAL ELEMENTS IMPACTING TRANSPORTER-SUBSTRATE BINDING INTERACTIONS

A thesis submitted in partial fulfillment of the requirements for the degree of Master of Science at Virginia Commonwealth University.

By

Julie Nguyen
Bachelor of Science, University of Virginia, Charlottesville, Virginia, 2019

Director: Douglas H. Sweet, Ph.D.
Professor,
Department of Pharmaceutics, School of Pharmacy

Virginia Commonwealth University
Richmond, Virginia
May, 2021

ACKNOWLEDGEMENTS

I would like to thank my advisor, Dr. Douglas Sweet, who has motivated and supported me in my journey towards completing my thesis project and obtaining my MS degree. Not only has he helped me grow as a scientist through hours of interpretation and discussion, Dr. Sweet has also gone above and beyond by being an unwavering source of encouragement. At times when experiments failed more often than they succeeded, deadlines were quickly approaching, and life seemed nothing short of a disaster in the making, Dr. Sweet was always there to listen and give sound advice. In the time I have spent working in Dr. Sweet's lab, I have learned the importance of challenging yourself intellectually, paying attention to the finer details, reflecting on mistakes, and maintaining a positive attitude. I cannot thank Dr. Sweet enough for providing me with the skills necessary to succeed in my future endeavors both academically and professionally.

To my research committee members, including Dr. Phillip Gerk and Dr. Keith Ellis, I thank you for your continuous feedback and suggestions on my research project. You challenged me to think critically about the technical aspects of my project. Additionally, you helped me gain a greater appreciation of the broader scope of my project in terms of its potential clinical application.

I thank VCU School of Pharmacy, particularly the Department of Pharmaceutics, for providing an educational environment that fosters both critical and creative thinking. To the Department of Pharmaceutics administrative staff, including Keyetta Tate, Laura Georgiadis, and Sha-Kim Craft, I sincerely thank you for your efforts to keep the department running smoothly.

I would like to extend my gratitude to my lab colleague, Dr. Christopher Jay, who showed me the ropes of the laboratory protocols and techniques that were integral to completing my research project.

Finally, a huge thank you goes out to my family and friends. Without their continued encouragement, faith, and love, I would have never been able to accomplish as much as I did. I owe my success to you, my stellar support group.

TABLE OF CONTENTS

LIST OF TABLES

LIST OF FIGURES

ABBREVIATIONS

ABC	ATP binding cassette
CHO	Chinese hamster ovary
DC	Dicarboxylate
DMEM/F12	Dulbecco's Modified Eagle/Ham's F-12 Medium
DMEM/HIGH GLUCOSE	Dulbecco's Modified Eagle Medium with high glucose
DNA	Deoxyribonucleic acid
EMA	European Medicines Agency
ES	Estrone sulfate
FDA	Food and Drug Administration
G418	Geneticin
HCl	Hydrochloric acid
HEK 293	Human embryonic kidney
HEPES	4-(2-hydroxyethyl)-1-piperazineethanesulfonic acid
hOAT	Human organic anion transporter
hOAT	Human organic anion transporter
K_m	Michaelis-Menten constant
LB	Luria broth
NaOH	Sodium hydroxide
NSAID	Non-steroidal anti-inflammatory drug
OAT	Organic anion transporter
PAH	*Para*-aminohippurate
PiPT	*Piriformospora indica* phosphate transporter

SLC	Solute carrier
TB	Transport buffer
TMD	Transmembrane domain
UV-Vis	Ultraviolet-visible
α-KG	α-ketoglutarate

ABSTRACT

HUMAN ORGANIC ANION TRANSPORTERS 1 AND 3: STRUCTURAL ELEMENTS IMPACTING TRANSPORTER-SUBSTRATE BINDING INTERACTIONS

By Julie Nguyen

Bachelor of Science, University of Virginia, Charlottesville, Virginia, USA

A thesis submitted in partial fulfillment of the requirements for the degree of Master of Science at Virginia Commonwealth University.

Virginia Commonwealth University, 2021

Director: Douglas H. Sweet, Ph.D.
Professor,
Department of Pharmaceutics, School of Pharmacy

Organic anion transporters (OATs) are known to interact with a wide variety of negatively charged drugs and can impact their clinical safety and efficacy profiles. The U.S. Food and Drug Administration (FDA) and European Medicines Agency (EMA) have recognized and highlighted the importance of evaluating the potential interactions with transporters, specifically hOAT1 and hOAT3, during the development of new drug entities. Little is known about OAT-drug interactions as they are difficult to discern on a molecular level in the absence of any solved crystal structures for OATs. Therefore, in a previous study, *in silico* homology models of hOAT1 and hOAT3 were generated based on the solved crystal structure for *Piriformospora indica* phosphate transporter (PiPT). The models were docked with their respective prototypical substrates, amino acid contacts involved in substrate recognition predicted, and single point mutations

generated. Following mutagenesis, singly mutated hOAT1 and hOAT3 transporters were subject to accumulation and saturation studies to determine their role in substrate binding and subsequent translocation. The findings from this previous study indicated singly mutated constructs did not result in altered binding affinity (K_m). However, the question remained whether these predicted amino acid contacts would significantly alter affinity when present in various double and triple combinations.

In this study, multiple combination hOAT1 (Arg15Lys/Ile19Leu, Ile19Leu/Tyr230Phe, Arg15Lys/Tyr230Phe, and Arg19Lys/Ile19Leu/Tyr230Phe) and hOAT3 mutants (Phe426Tyr/Phe430Ser and Phe426Tyr/Phe430Tyr) were generated and functional accumulation screens were conducted to determine the impact on overall transport activity. Mutants that retained transport activity were then further assessed by kinetic assays to determine any changes in K_m. Functional accumulation screens showed none of the hOAT1 multiple mutants retained PAH transport activity. In contrast, the generated hOAT3 double mutants retained ES transport activity. Subsequent kinetic analysis revealed the hOAT3 double mutants exhibited no statistically significant changes in estimated K_m values as compared to hOAT3 wild-type.

This study provides further insight as to the importance of these predicted critical amino acid residues in substrate binding interactions. Further characterizing these molecular interactions will allow for improved manipulation of drug substrate pharmacokinetics as well as prediction of drug-drug interactions, both of which can be utilized in drug design and development.

CHAPTER 1

1.A INTRODUCTION

Transporters have gained attention in the field of pharmacology as they are expressed throughout our bodies and play important roles in the absorption, distribution, and excretion of endogenous and exogenous substances, including drugs. There are two major superfamilies of membrane-bound transporters: ATP binding cassette (ABC) and solute carrier (SLC) transport proteins. ABC transporters directly bind and hydrolyze ATP to drive the translocation of substrates across the cell membrane. Whereas, SLCs are indirectly coupled to cellular energy and use ion gradients (e.g., symporters and antiporters) as well as electrochemical potential (e.g., facilitated diffusion) to drive transcellular transport of substrates (Figure 1.1) [11]. Among the 65 SLC families, the SLC22 family comprises anion/cation/zwitterion transporters [3,22,24]. Organic anion transporters (OATs) are a subtype of the SLC22 transport proteins that are responsible for the membrane translocation of negatively charged organic substrates such as toxins, nutrients, and drugs [14,16,22].

Twenty-nine transporters have been identified as potential members within the SLC22 family; many of which have been characterized in terms of transport mechanism, substrate and inhibition profiles, and tissue distribution [24]. Two of these members, OAT1 (SLC22A6) and OAT3 (SLC22A8), are further investigated in this project. OATs are proposed to have 12 alpha helical transmembrane domains (TMDs) with a large extracellular loop between TMDs 1 and 2, a large intracellular loop between TMDs 6 and 7, and cytosolic amino and carboxyl termini [9,17]. In humans, OAT1 and OAT3 share expression in the eye, brain, and kidneys while OAT1 and OAT3 are found in the placenta

and liver, respectively. Furthermore, they are highly expressed in the kidneys and targeted to the basolateral membrane of renal proximal tubule cells [15,20,21]. Additionally, they have high amino acid sequence similarity (50%) and are often expressed in the same cell types. Furthermore, while their specificities overlap, they often have different affinities for the same compound. This redundancy in substrate recognition may serve as an evolutionary survival mechanism that likely provides additional transport capacity in the following situations: 1) environmental exposure to toxic compounds, 2) drug-drug interactions, 3) genetic dysfunction (e.g., gene variants), and 4) pathophysiological states (e.g., renal insufficiency) [23]. In renal proximal tubule cells, human OAT1 (hOAT1) and OAT3 (hOAT3) are specifically responsible for mediating the absorption of organic anion substrates from the blood across the cell membrane via a dicarboxylate/organic anion antiport mechanism (Figure 1.1) [11,22]. Prototypical substrates for hOAT1 (*para*-aminohippurate, or PAH) and hOAT3 (estrone sulfate, or ES) are exchanged for α-ketoglutarate (α-KG), the only known physiological counterion. Efflux of substrates occurs through facilitated diffusion carriers and/or efflux transporters.

In addition to the prototypical substrates, hOAT1 and hOAT3 bind to a wide variety of structurally diverse negatively charge compounds under physiological conditions (i.e., pH 7.4) including NSAIDs (e.g., indomethacin), antivirals (e.g., acyclovir), β-lactam antibiotics (e.g., penicillin), diuretics (e.g., furosemide), and chemotherapeutic agents (e.g., cisplatin) [4,5,6]. OATs impact the pharmacokinetics and pharmacodynamics of several dozens of drugs, potentially altering their clinical safety and efficacy profiles. Both the U.S. Food and Drug Administration (FDA) and the European Medicines Agency (EMA) have issued guidances that recognize the importance of *in vitro* studies of

investigational new drugs to be evaluated as potential substrates or inhibitors for transporters known to be involved in drug interactions [1,7,13]. These guidances specifically identify hOAT1 and hOAT3 as transporters that need to be evaluated for potential interactions with the new chemical entity and to determine if further *in vivo* studies are required regarding potential drug-drug interactions [1,7,13]. Thereby, highlighting the importance of studying the structure-activity relationship of hOAT1 and hOAT3 in drug substrate binding interactions.

As several substances are known to interact with hOAT1 and hOAT3 for renal elimination, gaining a better understanding of the biochemical binding mechanisms of OATs is vital to predict their pharmacokinetics as well as therapeutic safety and efficacy. Doing so potentially allows transporter-substrate interactions to be manipulated to maximize efficacy and minimize renal toxicity [12]. For example, renal elimination can be slowed by optimizing transporter-drug interactions to decrease binding affinity. This may be used to improve the therapeutic effects of a poorly bioavailable drug as well as to lower its dosage or dosing frequency. Furthermore, generating compounds that have greater specificity for a transporter and are co-formulated as excipients (e.g., probenecid) may decrease drug-drug interactions and/or allow for preferential competitive binding at target transporters [12]. Ultimately, identifying and characterizing critical amino acids involved in substrate recognition for hOAT1 and hOAT3 may offer great insight into drug design to control pharmacokinetics as well as to better predict drug-drug interactions.

The lack of structural information (i.e., no solved crystal structure) for OATs has made it challenging to understand these molecular interactions [17]. In order to study substrate binding via hOAT1 and hOAT3, *in silico* homology models of each transporter

were previously generated based on the solved crystal structure of *Piriformospora indica* phosphate transporter (PiPT) [8]. Substrates were docked and from these models amino acids potentially critical to binding interactions were determined (Figure 1.2 and Figure 1.3). Subsequently, single mutants were generated (Table 1.1 and Table 1.2) and screened for transport activity [8]. Initial accumulation studies revealed hOAT1 substitutions Arg15Lys, Ile19Leu, and Tyr230Phe and hOAT3 substitutions Phe426Tyr, Phe430Ser, and Phe430Tyr retained sufficient transport activity to pursue saturation analyses. For hOAT1, saturation analyses showed none of the single mutants had significantly altered affinity (K_m) compared to wild-type. For hOAT3, one single mutant (Phe430Ser) showed significantly altered K_m compared to wild-type suggesting weaker binding affinity. These findings suggest that a single mutation is insufficient to significantly impact affinity, however double or triple combinations of these mutants could potentially have a greater impact on substrate binding and transport kinetics. Thus, in this project, we explored the hypothesis that multiple mutant combinations are needed to significantly alter hOAT1 and hOAT3 substrate binding affinity through the following specific aims:

1.B SPECIFIC AIMS

Specific Aim 1

To test the hypothesis that double and triple combinations of point mutants at predicted critical substrate binding contacts will result in altered substrate binding affinity for hOAT1, we:

a. Generated double/triple mutants using site-directed mutagenesis.
b. Established stably transfected cell lines expressing hOAT1 mutants.
c. Identified active and inactive mutants via substrate accumulation assays.
d. Determined the binding affinity of active mutants and their prototypical substrate PAH.

Specific Aim 2

To test the hypothesis that double and triple combinations of point mutants at predicted critical substrate binding contacts will result in altered substrate binding affinity for hOAT3, we:

a. Generated double mutants using site-directed mutagenesis.
b. Established stably transfected cell lines expressing hOAT3 mutants.
c. Identified active and inactive mutants via substrate accumulation assays.
d. Determined the binding affinity of active mutants and their prototypical substrate ES.

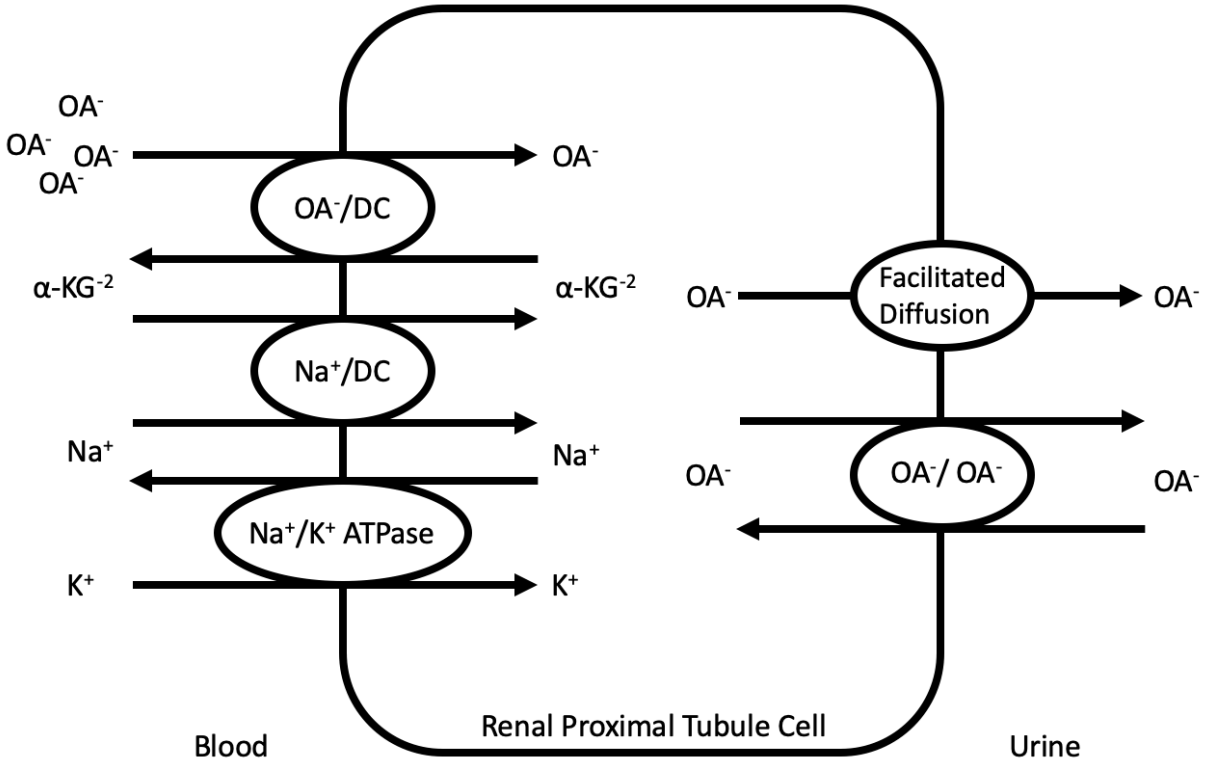

Figure 1.1. Model depicting driving forces for OAT1 and OAT3 transport.
Mechanisms/driving forces used for cellular entry and exit for organic anion transport using renal proximal tubule cell as an example.

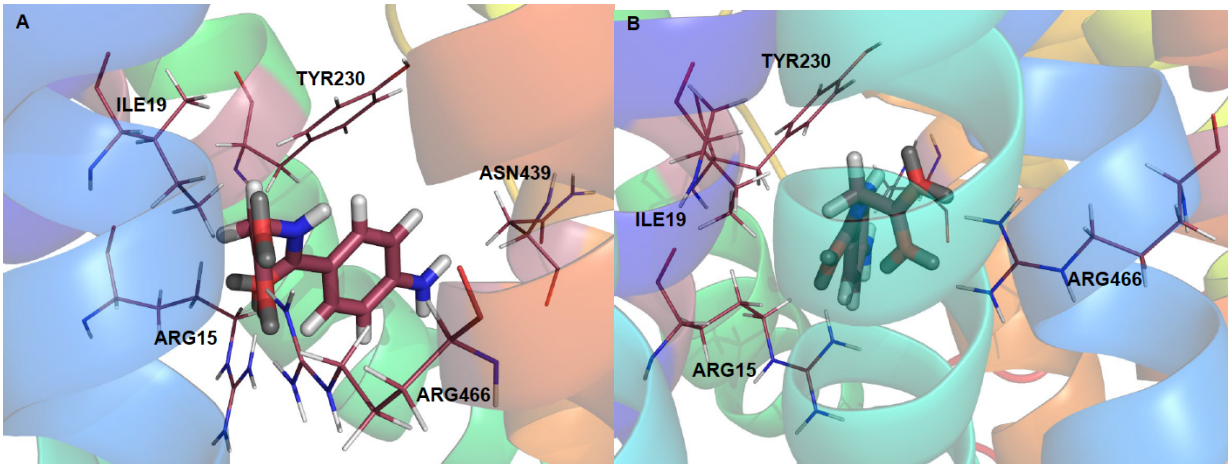

Figure 1.2. Different rotational views of the hOAT1-PAH binding complex.
The five amino acids predicted to be important for PAH binding and transport are indicated. Image files generated using PyMOL 1.8.

[Figure taken from reference [8]]

Table 1.1. Summary of putative PAH-hOAT1 complex forming amino acids, the predicted nature of each interaction and generated conservative and non-conservative hOAT1 mutations.

TMD	Amino Acid	Interaction	Conservative	Non-conservative
1	Arg15	Hydrogen Bond	Lys	Ala
1	Ile19	Hydrophobic	Leu	Ala
5	Tyr230	Edge-Face Aromatic	Phe	Ala
10	Asn439	Hydrogen Bond	Gln	Ala
11	Arg466	Salt Bridge featuring Bidentate Hydrogen Bond	Lys	Ala

[Table taken from reference [8]]

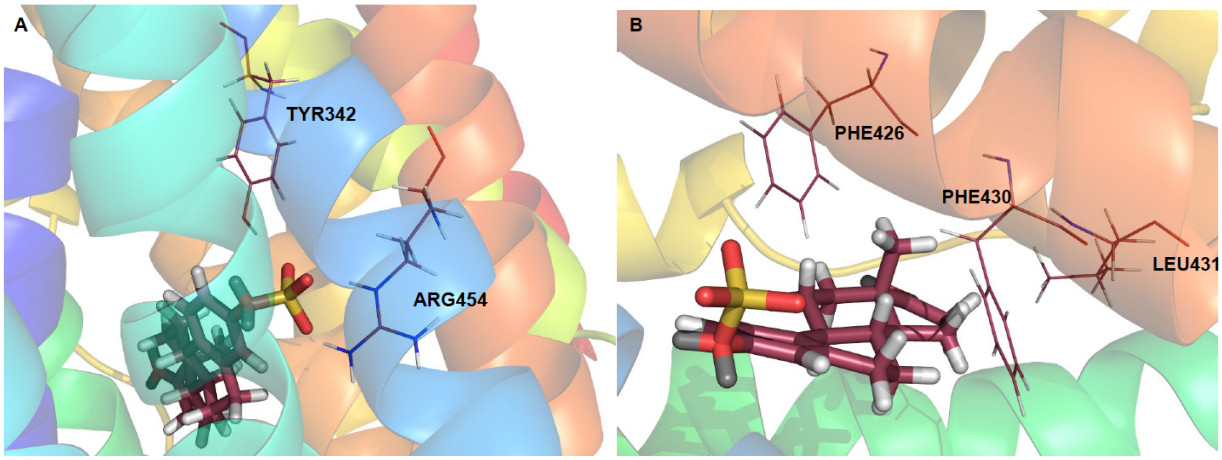

Figure 1.3. Different rotational views of the hOAT3-ES binding complex.
The five amino acids predicted to be important for ES binding and transport are indicated. Image files generated using PyMOL 1.8.

[Figure taken from reference [8]]

Table 1.2. Summary of putative ES-hOAT3 complex forming amino acids, the predicted nature of each interaction and generated conservative and non-conservative hOAT3 mutations.

TMD	Amino Acid	Interaction	Conservative	Non-conservative
7	Tyr342	Edge-Face Aromatic	Phe	Ala
10	Phe426	Hydrophobic	Tyr	Ser
10	Phe430	Hydrophobic	Tyr	Ser
10	Leu431	Hydrophobic	Ile	Ala
11	Arg454	Salt Bridge featuring Bidentate Hydrogen Bond	Lys	Ala

[Table taken from reference [8]]

CHAPTER 2

IDENTIFYING STRUCTURAL ELEMENTS OF HUMAN ORGANIC ANION TRANSPORTERS 1 AND 3 MEDIATING SUBSTRATE-TRANSPORTER BINDING INTERACTIONS

2.A INTRODUCTION

Previously studied hOAT1 and hOAT3 transport active single mutants were combined to generate double and/or triple mutants. Multiple combination mutants were stably expressed in CHO or HEK cells in order to determine retention of transport function. Functional screening indicated none of the hOAT1 mutants, but both of the hOAT3 double mutants (Phe426Tyr/Phe430Ser and Phe436Tyr/Phe430Tyr) exhibited significant changes in substrate accumulation as compared to parental cells. Saturation analysis of transport active hOAT3 double mutants indicated no change in affinity as compared to hOAT3 wild-type.

2.B MATERIALS AND METHODS

2.B.1 Chemicals and Reagents

Mutagenesis and sequencing primers were purchased from Integrated DNA Technologies (Coralville, IA). The QuikChange Lightning Site-Directed Mutagenesis Kit and DH5-α cells were purchased from Agilent Technologies (Santa Clara, CA). hOAT3 mutants were purchased from GenScript. Lipofectamine transfection reagents, Dulbecco's Modified Eagle/Ham's F-12 Medium (DMEM/F12), and Dulbecco's Modified Eagle Medium with high glucose (DMEM/HIGH GLUCOSE) were purchased from Thermo

Fisher Scientific (Waltham, MA). QIAprep spin miniprep kits were purchased from QIAGEN (Germantown, MD). Geneticin (G418) and Penicillin-Streptomycin were purchased from Gibco-Invitrogen (Grand Island, NY). [H^3] PAH was purchased from PerkinElmer Life and Analytical Science (Waltham, MA). Unlabeled PAH and probenecid were purchased from Sigma-Aldrich (St. Louis, MO). Ecoscint H cocktail was purchased from National Diagnostics (Atlanta, GA). Bradford protein assay dye was purchased from Bio-Rad Laboratories. GoTaq green master mix was purchased from Promega (Madison, WI).

2.B.2 hOAT1 Mutant Generation

Using previously constructed hOAT1 single point mutants as template, hOAT1 double and triple combination mutants were constructed using the QuikChange Lightning Site-Directed Mutagenesis Kit according to the manufacturer's recommendations [2]. Briefly, the single mutant template (for double combination mutants) or the double mutant template (for triple combination mutant) was denatured, primers annealed to the template to introduce the additional desired mutation(s), and the mutant DNA strand elongated. Samples were incubated with Dpn1 restriction enzyme to degrade hOAT1 wild-type template strands. Oligonucleotide primers containing the desired mutations are reported in Table 2.1.

2.B.3 hOAT3 Mutant Generation

Multiple attempts at generating hOAT3 double combination mutants with the previously described method for hOAT1 were unsuccessful. Following reanalysis of the desired mutation positions, it was discovered there was wild-type sequence in the mutagenesis primers that overlapped mutant sequence in the template. Therefore,

primers that would introduce both desired mutations at once were generated to construct hOAT3 double mutants. After these generation attempts failed, hOAT3 double mutants were synthesized by GenScript in order to move forward with subsequent experimentation. Sequences used to generate the desired hOAT3 mutants are reported in Table 2.2.

Table 2.1. Oligonucleotide primers used for hOAT1 site-directed mutagenesis.

Template	Mutagenesis Position	Substitution	Primers (5' - 3')	Final Mutant
R15K	19	Isoleucine → Leucine	Forward CCGCTTCCAGCAG**TTG**CAGGTCACCCTGG Reverse CCAGGGTGACCTG**CAA**CTGCTGGAAGCGG	R15K/I19L
I19L	230	Tyrosine → Phenylalanine	Forward GGGCACCTTGATTGGCTATGTC**TTT**AGCCTGGGCCAG Reverse CTGGCCCAGGCT**AAA**GACATAGCCAATCAAGGTGCCC	I19L/Y230F
R15K	230	Tyrosine → Phenylalanine	Forward GGGCACCTTGATTGGCTATGTC**TTT**AGCCTGGGCCAG Reverse CTGGCCCAGGCT**AAA**GACATAGCCAATCAAGGTGCCC	R15K/Y230F
R15K/I19L	230	Tyrosine → Phenylalanine	Forward GGGCACCTTGATTGGCTATGTC**TTT**AGCCTGGGCCAG Reverse CTGGCCCAGGCT**AAA**GACATAGCCAATCAAGGTGCCC	R15K/I19L/Y230F

Table 2.2. hOAT3 site-directed mutagenesis.

Template	Mutagenesis Position	Substitution	Sequence Substitution	Final Mutant
Wild-type	426 & 430	426: Phenylalanine → Tyrosine 430: Phenylalanine → Serine	Forward CCTATCCAGCTCC**TAC**AGCTGCCTC**TCC**CTCTACACAAGT Reverse ACTTGTGTAGAG**GGA**GAGGCAGCT**GTA**GGAGCTGGATAGG	F426Y/F430S
Wild-type	426 & 430	426: Phenylalanine → Tyrosine 430: Phenylalanine → Tyrosine	Forward CCTATCCAGCTCC**TAC**AGCTGCCTC**TAC**CTCTACACAAGT Reverse ACTTGTGTAGAG**GTA**GAGGCAGCT**GTA**GGAGCTGGATAGG	F426Y/F430Y

2.B.4. Bacterial Transformation

hOAT1 and hOAT3 mutant plasmids were transformed into XL10-Gold Ultracompetent and DH5-α cells, respectively, according to the manufacturer's protocol [2]. Transformed bacterial cells were spread on LB agar plates containing ampicillin (0.1 mg/mL) and incubated at 37°C for 16 hrs. Individual colonies were picked and incubated for 16 hrs in 5 mL LB broth containing 0.1 mg/mL ampicillin at 37°C while being shaken at 225 RPM.

2.B.5 Mutant Confirmation

Plasmid DNA from the overnight culture was isolated and purified using QIAGEN's Mini-Prep Kit following the manufacturer's protocol [18]. Briefly, bacterial cultures were pelleted, resuspended, lysed, neutralized, and centrifuged at 13,000 RPM for 10 min. The supernatant was applied to the spin columns where plasmid DNA binds to, and contaminating material is washed from, the column. Following elution of the purified plasmid DNA from the column, DNA concentration and purity were determined using UV-Vis spectroscopy. hOAT1 and hOAT3 mutants were confirmed by DNA sequencing (Genewiz, South Plainfield, NJ) with the primers in Table 2.3 and Table 2.4, respectively. The presence of the desired mutations was confirmed by comparing sequence files and chromatograms for the mutants against hOAT1 and hOAT3 wild-type.

Table 2.3. Oligonucleotide primers used for hOAT1 DNA sequencing.

Primer	Primer Sequence (5' - 3')
hOAT1 Forward 1	CCCATCTACCATCGTGACTG
hOAT1 Forward 2	AGTCTGCAGAAGGAGCTGAC
hOAT1 Reverse 1	CATTGAGCAGGATGCAGATG
hOAT1 Reverse 2	AAGTTGGGTGCGAAGGCTGC
T7	TAATACGACTCACTATAGGG
BGHR	TAGAAGGCACAGTCGAGG

Table 2.4. Oligonucleotide primers used for hOAT3 DNA sequencing.

Primer	Primer Sequence (5' - 3')
hOAT3 Forward 1	TGGTCTTCCGCTTCCTGTG
hOAT3 Forward 2	CTTAAGCTACCTGGGCC
hOAT3 Reverse 1	CTAGGATCAGTCTCTGGAGG
hOAT3 Reverse 2	CCTCCGAGGACTTTCCAGAC
T7	TAATACGACTCACTATAGGG
BGHR	TAGAAGGCACAGTCGAGG

2.B.6 Transfection and Cell Culture

Stable Chinese hamster ovary (CHO) and human embryonic kidney (HEK 293) cell lines expressing confirmed mutant transporters were generated for hOAT1 and hOAT3, respectively, using cationic lipid-based transfection according to the Lipofectamine 2000 Reagent protocol [10]. Briefly, 1 µg plasmid DNA and 4 µL Lipofectamine 2000 were mixed, diluted with OptiMEM, and applied to cells at 70-80% confluency in 12-well tissue culture plates. Prior to seeding for hOAT3 mutant transfections, tissue culture plates were coated with 0.1 mg/mL poly-D-lysine. Fresh DMEM/F12 and DMEM/HIGH GLUCOSE containing 10% FBS was added to each well for hOAT1 and hOAT3 mutant transfections, respectively, prior to adding the plasmid DNA/Lipofectamine 2000/OptiMEM mixture. After incubating for 24 to 48 hrs at 37°C with 5% CO_2, the transfection medium was replaced with fresh medium containing G418 (1mg/mL) for 2 to 3 weeks of antibiotic selection. Cells viable in the presence of G418 were moved to culture flasks and maintained under antibiotic selective pressure (0.25 mg/mL G418). All CHO and HEK 293 cells lines were maintained in DMEM/F12 and DMEM/HIGH GLUCOSE, respectively, containing 10% FBS, 1% Penicillin-Streptomycin, and 0.25 mg/mL G418 (for transporter expressing cell lines) at 37°C with 5% CO_2. Cells were subcultured once they reached 80-90% confluency.

2.A.7 Accumulation Assay Screen

Generated mutants were tested for transport activity via cell accumulation assays. Briefly, cells were seeded in 24-well tissue culture plates at 250,000 cells/well in the absence of antibiotics 48 hrs before the experiment. For all assays involving HEK 293 cells, tissue culture plates were coated with 0.1 mg/mL poly-D-lysine. Culture medium

was removed and cells were equilibrated at room temperature for 10 min with 500 µL transport buffer (TB). Cells were incubated in 400 µL TB containing 5 µM PAH (or ES) spiked with 0.25 µCi/mL [H^3] PAH (or [H^3] ES) in the presence or absence of the inhibitor probenecid (500 µM). After a 10 min incubation, treatment was removed and cells were immediately washed three times with ice-cold TB. Cells were lysed with 200µL 1N NaOH, neutralized with 250 µL 1N HCl, and 200 µL 10 mM HEPES. Radioactivity in cell lysates was quantified by liquid scintillation counting using 400 µL of sample and 5 mL Ecoscint H cocktail. Substrate accumulation was determined from background corrected counts and normalized by the protein content as determined via a Bradford protein assay using 10 µL of sample and 200 µL protein assay dye. Accumulation values were corrected for background accumulation (diffusion) in parental CHO and HEK 293 cells via linear regression (Y = mX+b) as appropriate. Initial activity screen values were reported as average ± SD from triplicate samples.

2.B.8 Kinetic Assay

The Michaelis-Menten constant (K_m) was determined for PAH and ES on active hOAT1 and hOAT3 mutants, respectively, via saturation analysis. Mutant expressing cells were seeded in 24-well tissue culture plates at 250,000 cells/well in the absence of antibiotics 48 hrs before the experiment. For all assays involving HEK 293 cells, tissue culture plates were coated with 0.1 mg/mL poly-D-lysine. Culture medium was removed and cells were equilibrated at room temperature for 10 min with 500µL TB. Cells were incubated in 400 µL TB containing increasing concentration of PAH (1-200 µM PAH or ES) spiked with 0.25 µCi/mL [H^3] PAH (or [H^3] ES). After a 1 min incubation, treatment was removed and cells were immediately washed three times with ice-cold TB. Cells were

lysed with 200 µL 1N NaOH, neutralized with 250 µL 1N HCl, and 200 µL 10 mM HEPES. Radioactivity in cell lysates was quantified by liquid scintillation counting using 400 µL of sample and 5 mL Ecoscint H cocktail. Substrate accumulation was determined from background corrected counts and normalized by the protein content as determined via a Bradford protein assay using 10 µL of sample and 200 µL protein assay dye. Accumulation values were corrected for background accumulation (diffusion) in parental CHO and HEK 293 cells via linear regression (Y = mX+b) as appropriate. Transporter mediated uptake was plotted and analyzed using nonlinear regression (Y = Vmax*X/(Km + X)) in GraphPad Prism (GraphPad Software Inc., San Diego, CA) to generate K_m estimates. K_m estimates from individual experiments were reported as average ± SD from triplicate samples. Final K_m estimates from at least two independent experiments were reported as average ± SE.

2.B.9 Statistics

Data are plotted as average ± SD for initial screen and saturation assays. One-way ANOVA with post-hoc Dunnett's multiple comparisons were used to determine differences compared to a single control for initial screens. Differences were considered statistically significant if $p < 0.05$. Final K_m estimates are reported as average ± SE. GraphPad Prism version 9.1.0 was used for statistical analysis.

2.C RESULTS

2.C.1 hOAT Mutant DNA Confirmation

All hOAT1 and hOAT3 mutant constructs were confirmed by DNA sequencing. Figure 2.1 shows chromatograms for the hOAT1 Arg15Lys/Ile19Leu double mutants. In Figure 2.1A, the hOAT1 Arg15Lys single mutant template sequence shows an AAG codon for lysine at position 15 and an ATC codon for isoleucine at position 19. In Figure 2.1B, the mutated TTG codon for leucine is observed. Figure 2.2 shows chromatograms for the hOAT1 Ile19Leu/Tyr230Phe double mutant. In Figure 2.2A, the hOAT1 Ile19Leu single mutant template sequence shows a TTG codon for leucine at position 19 and a TAC codon for tyrosine at position 230. In Figure 2.2B, the mutated TTT codon for phenylalanine is observed. Figure 2.3 shows chromatograms for the hOAT1 Arg15Lys/Tyr230Phe double mutant. In Figure 2.3A, the hOAT1 Arg15Lys single mutant template sequence shows an AAG codon for lysine at position 15 and a TAC codon for tyrosine at position 230. In Figure 2.3B, the mutated TTT codon for phenylalanine is observed. Figure 2.4 shows chromatograms for the hOAT1 Arg15Lys/Ile19Leu/Tyr230Phe triple mutant. In Figure 2.4A, the hOAT1 Arg15Lys/Ile19Leu double mutant template sequence shows an AAG codon for lysine at position 15, a TTG for leucine at position 19, and a TAC for tyrosine at position 230. In Figure 2.4B, the mutated TTT codon for phenylalanine is observed.

Figure 2.5 shows chromatograms for the hOAT3 double mutants generated. In Figure 2.5A, the hOAT3 wild-type template sequence shows a TTC codon for phenylalanine at positions 426 and 430. In Figure 2.5B, the mutated TAC codon for tyrosine and TCC codon for serine at positions 426 and 430, respectively, are observed.

In Figure 2.5C, the mutated TAC codons for tyrosine are observed at positions 426 and 430.

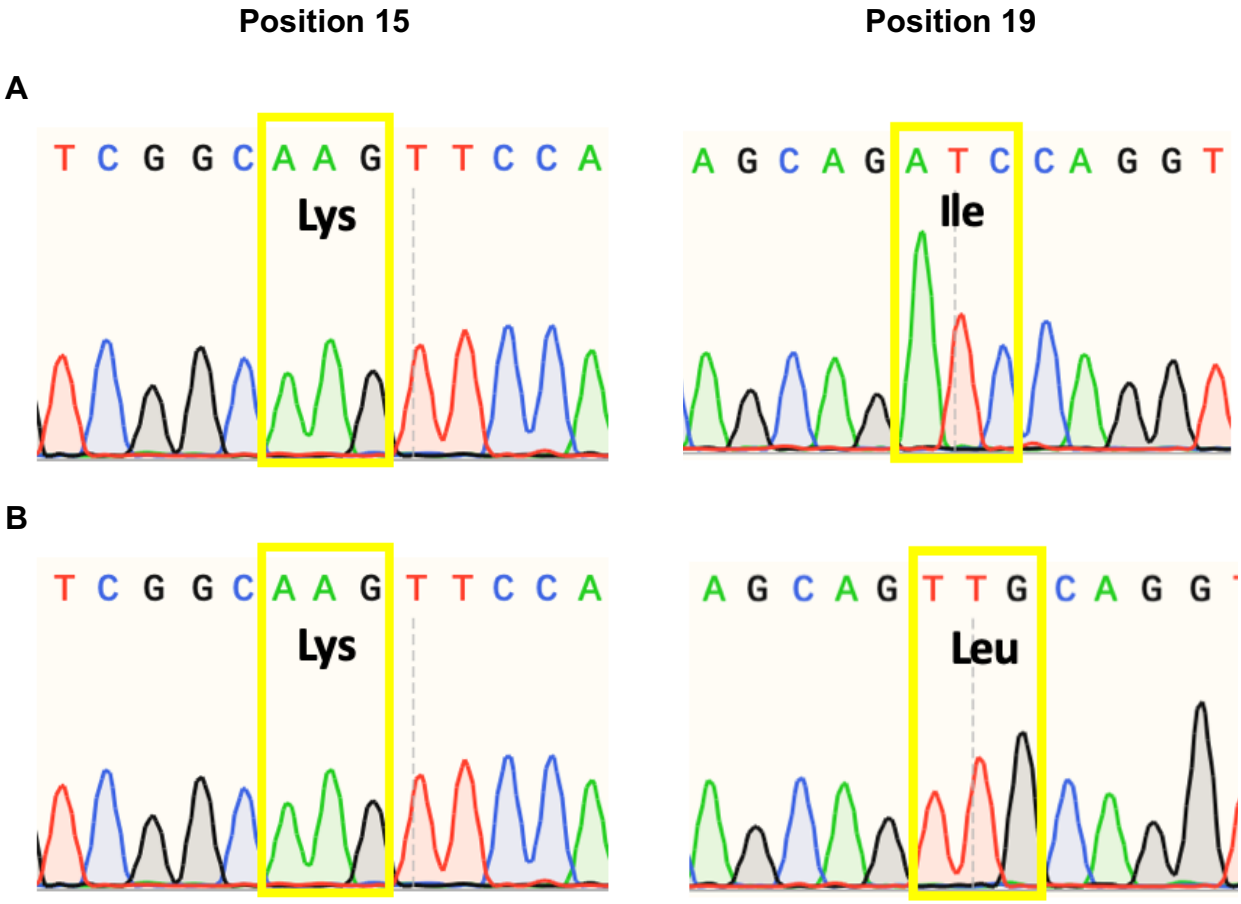

Figure 2.1. Chromatograms for DNA sequencing confirmation of hOAT1 Arg15Lys/Ile19Leu double mutant.
The chromatograms for hOAT1 Arg15Lys single mutant **(A)** and hOAT1 Arg15Lys/Ile19Leu double mutant **(B)** DNA sequence. Arg15Lys was used as a template and position 19 was mutated. The highlighted regions show the mutated position as well as the amino acid that is translated as a result.

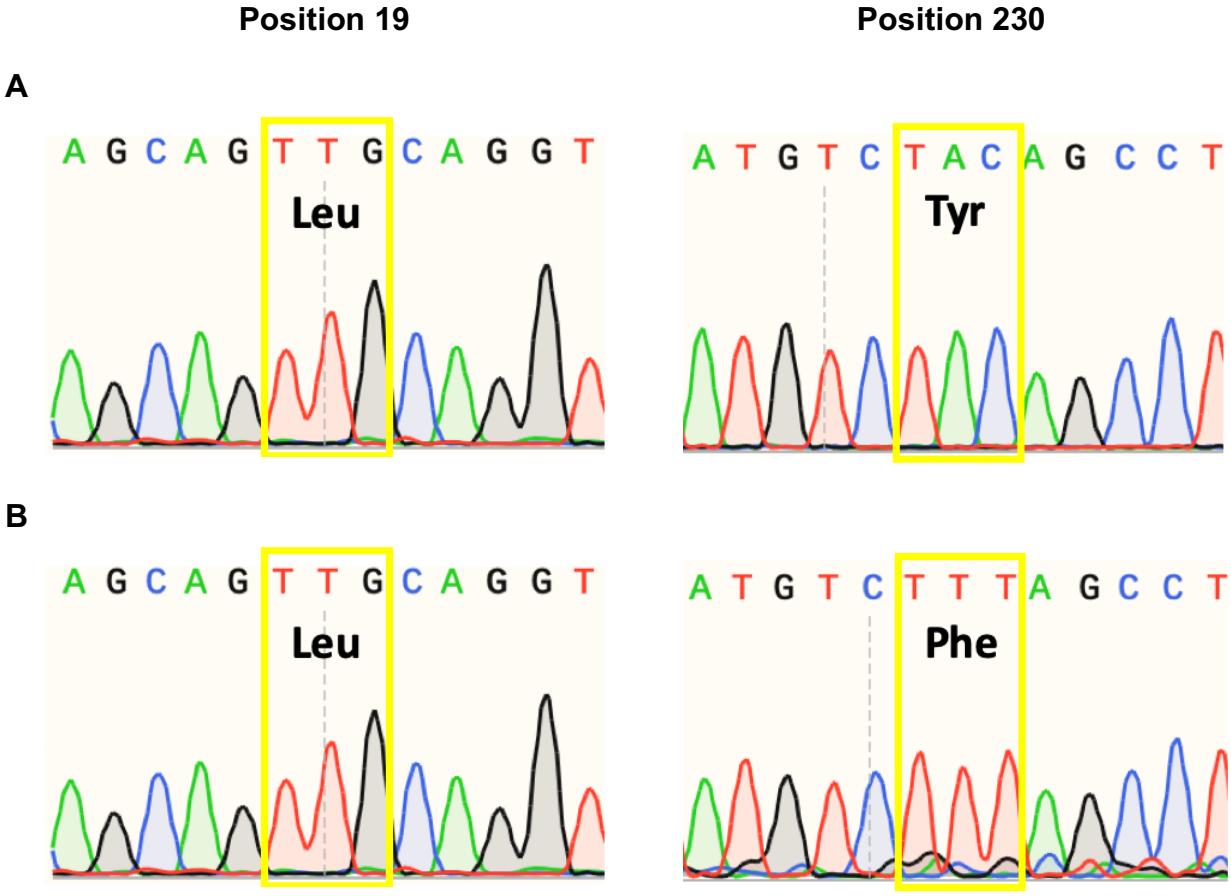

Figure 2.2. Chromatograms for DNA sequencing confirmation of hOAT1 Ile19Leu/Tyr230Phe double mutant.
The chromatograms for hOAT1 Ile19Leu single mutant **(A)** and hOAT1 Ile19Leu/Tyr230Phe double mutant **(B)** DNA sequence. Ile19Leu was used as a template and position 230 was mutated. The highlighted regions show the mutated position as well as the amino acid that is translated as a result.

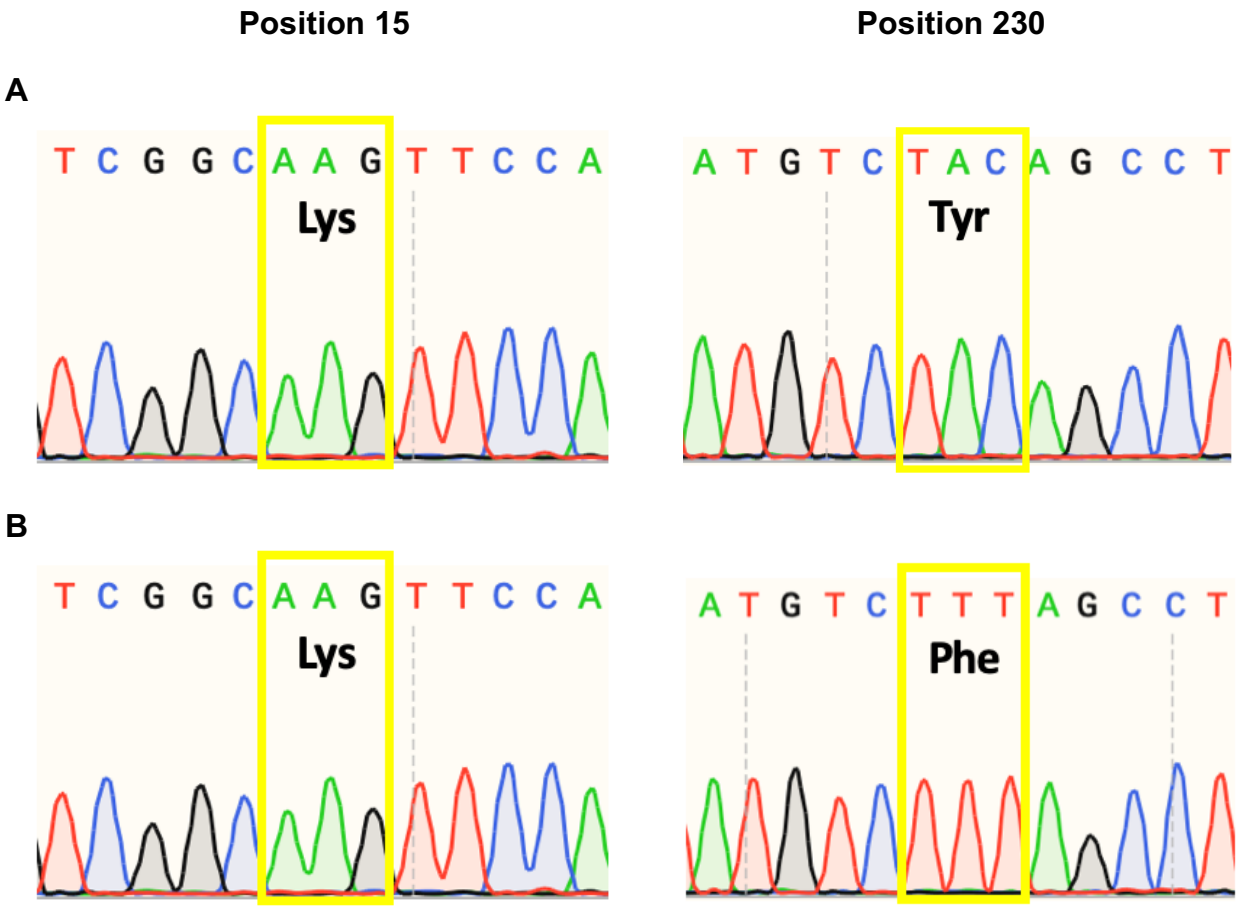

Figure 2.3. Chromatograms for DNA sequencing confirmation of hOAT1 Arg15Lys/Tyr230Phe double mutant.
The chromatograms for hOAT1 Arg15Lys single mutant **(A)** and hOAT1 Arg15Lys/Tyr230Phe double mutant **(B)** DNA sequence. Arg15Lys was used as a template and position 230 was mutated. The highlighted regions show the mutated position as well as the amino acid that is translated as a result.

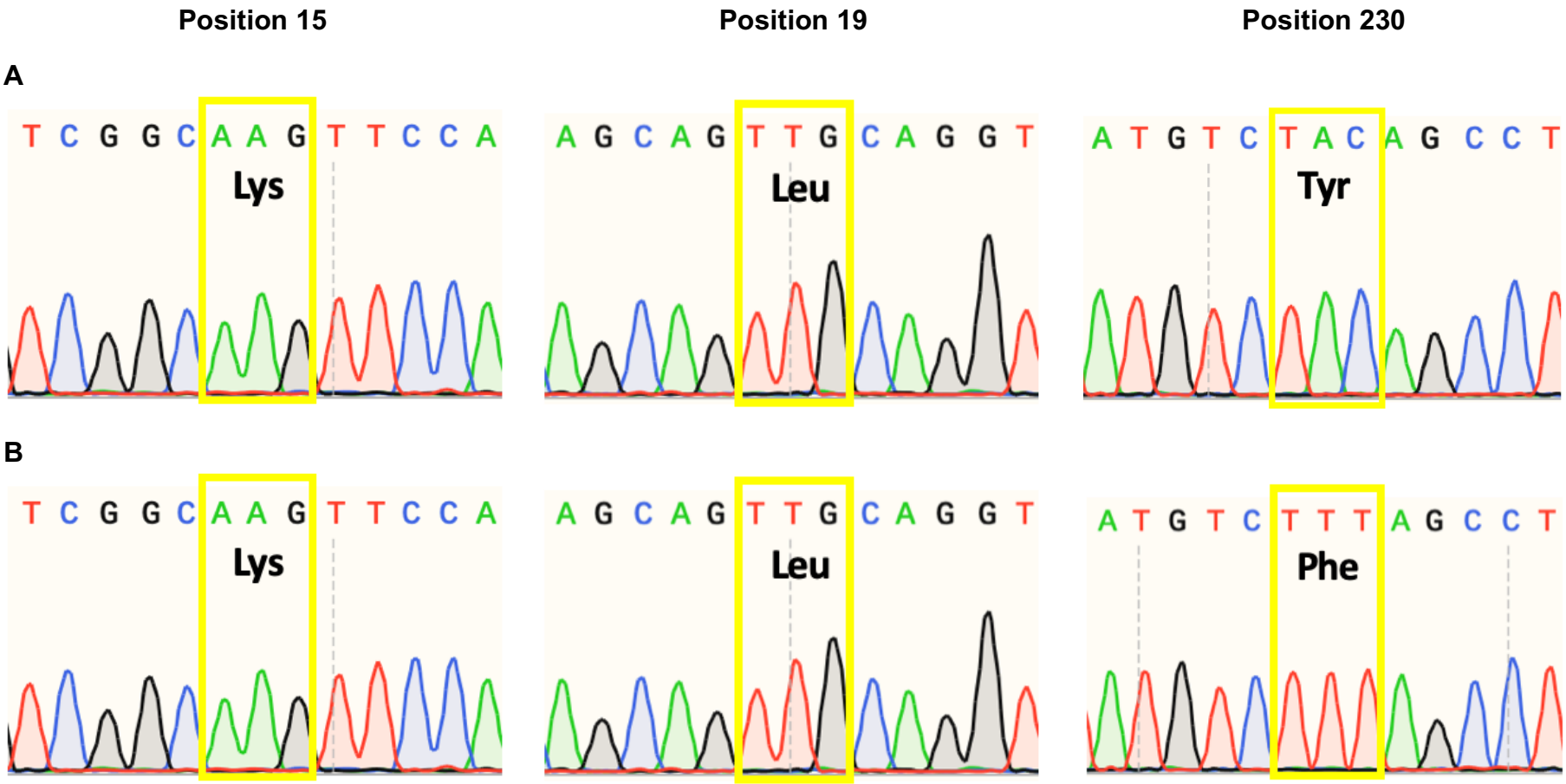

Figure 2.4. Chromatograms for DNA sequencing confirmation of hOAT1 Arg15Lys/Ile19Leu/Tyr230Phe triple mutant.

The chromatograms for hOAT1 Arg15Lys/Ile19Leu double mutant **(A)** and hOAT1 Arg15Lys/Ile19Leu/Tyr230Phe triple mutant **(B)** DNA sequence. Arg15Lys/Ile19Leu was used as a template and position 230 was mutated. The highlighted regions show the mutated position as well as the amino acid that is translated as a result.

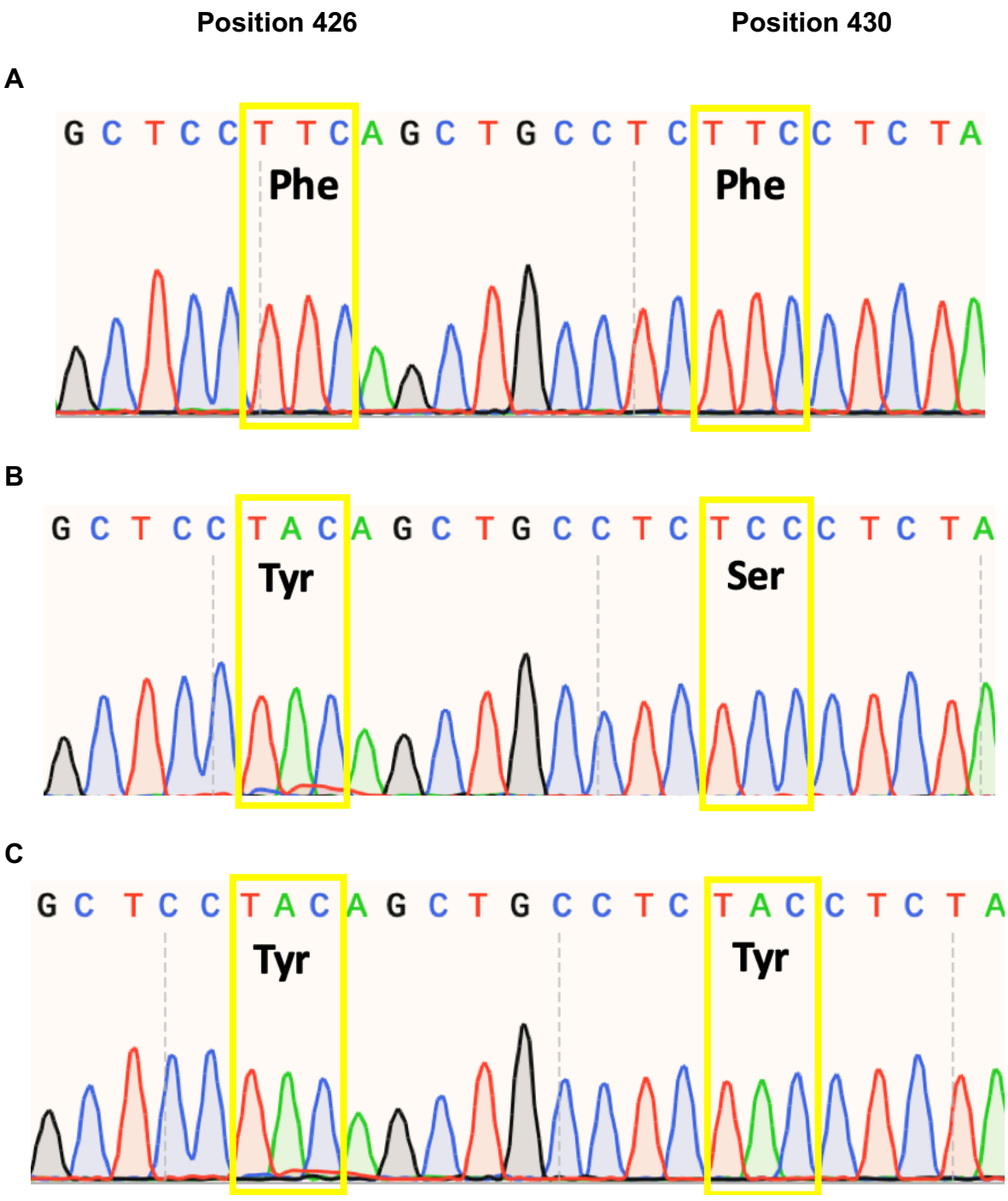

Figure 2.5. Chromatograms for DNA sequencing confirmation of hOAT3 double mutants.
The chromatograms for hOAT3 wild-type **(A)**, hOAT3 Phe426Tyr/Phe430Ser double mutant **(B)**, and hOAT3 Phe426Tyr/Phe430Tyr double mutant **(C)** DNA sequence. hOAT3 wild-type was used as a template and positions 426 and 430 were mutated. The highlighted regions show the mutated position as well as the amino acid that is translated as a result.

2.C.2 Accumulation Assay Screen

Accumulation assays were performed with stably-expressing cell lines to determine overall transport activity of cells expressing wild-type and mutant hOAT1 (Figure 2.6 and Figure 2.7) and hOAT3 (Figure 2.8). Initially, only one functional screen for hOAT1, which will be referred to as "Round 1 functional screen", was used to determine transport activity and inactivity of the hOAT1 mutants (Figure 2.6). In Figure 2.6, hOAT1 wild-type cells (113.0 ± 2.6 pmol/mg protein/10 min) showed significant PAH accumulation approximately 31 fold higher than CHO parental cells (3.6 ± 2.7 pmol/mg protein/10 min). PAH accumulation in the probenecid exposed hOAT1 wild-type cells (7.8 ± 2.7 pmol/mg protein/10 min) is comparable to that of the CHO parental cells (3.6 ± 1.5 pmol/mg protein/10 min), demonstrating nearly complete inhibition of transport activity. A one-way ANOVA with Dunnett's multiple comparison test between hOAT1 mutants and CHO parent were performed to determine whether hOAT1 mutants were active or inactive. hOAT1 mutants Arg15Lys/Ile19Leu (18.1 ± 6.6 pmol/mg protein/10 min) and Ile19Leu/Tyr230Phe (15.2 ± 3.5 pmol/mg protein/10 min) appeared to retain PAH transport activity and were statistically different from CHO parent ($p < 0.05$), suggesting these two are transport active mutants. PAH accumulation in hOAT1 mutants Arg15Lys/Tyr230Phe (9.9 ± 2.2 pmol/mg protein/10 min) and Arg15Lys/Ile19Leu/Tyr230Phe (7.1 ± 3.5 pmol/mg protein/10 min) were not statistically different from CHO parent, indicating they are transport inactive mutants.

Due to lack of transport activity observed (as described below in Kinetic Assays), a second accumulation assay (Figure 2.7), which is referred to as "Round 2 functional screen" was done to reassess active and inactive hOAT1 mutants. In Figure 2.7, hOAT1

wild-type cells (21.8 ± 1.1 pmol/mg protein/10 min) showed significant PAH accumulation approximately seven-fold higher than CHO parental cells (3.2 ± 0.3 pmol/mg protein/10 min). PAH accumulation in the probenecid exposed hOAT1 wild-type cells (4.0 ± 0.6 pmol/mg protein/10 min) is comparable to that of the CHO parental cells (3.1 ± 0.9 pmol/mg protein/10 min), demonstrating nearly complete inhibition of transport activity. hOAT1 mutants Arg15Lys/Ile19Leu (4.3 ± 0.4 pmol/mg protein/10 min), Ile19Leu/Tyr230Phe (4.3 ± 0.2 pmol/mg protein/10 min), Arg15Lys/Tyr230Phe (4.7 ± 0.2 pmol/mg protein/10 min), and Arg15Lys/Ile19Leu/Tyr230Phe (5.2 ± 1.1 pmol/mg protein/10 min) did not retain significant PAH transport activity as compared to CHO parent. A one-way ANOVA with Dunnett's multiple comparison test between hOAT1 mutants and CHO parent was performed to determine whether hOAT1 mutants were active or inactive. Only one hOAT1 mutant (Arg15Lys/Ile19Leu/Tyr230Phe) was statistically different from CHO parent ($p < 0.05$). Although, Arg15Lys/Ile19Leu/Tyr230Phe was statistically different from CHO parent, it was ultimately considered inactive because PAH accumulation in Arg15Lys/Ile19Leu/Tyr230Phe was comparable in the presence (3.6 ± 0.5 pmol/mg protein/10 min) and absence (5.3 ± 1.1 pmol/mg protein/10 min) of probenecid, indicating there was no inhibitable transport activity (as described below in Discussion). All hOAT1 mutants were considered transport inactive according to the Round 2 functional screen.

In Figure 2.8, hOAT3 wild-type cells (399.6 ± 2.7 pmol/mg protein/10 min) showed significant ES accumulation approximately nine-fold higher than HEK 293 parental cells (42.6 ± 25.2 pmol/mg protein/10 min). ES accumulation in the probenecid exposed hOAT3 wild-type cells (14.1 ± 4.1 pmol/mg protein/10 min) is comparable to that of the

HEK 293 parental cells (19.0 ± 7.8 pmol/mg protein/10 min), demonstrating nearly complete inhibition of transport activity. hOAT3 mutants Phe426Tyr/Phe430Ser (234.4 ± 30.0 pmol/mg protein/10 min) and Phe426Tyr/Phe430Tyr (366.0 ± 20.2 pmol/mg protein/10 min) retained statistically significant ES transport activity compared to HEK 293 parent ($p < 0.0001$) and were considered transport active mutants.

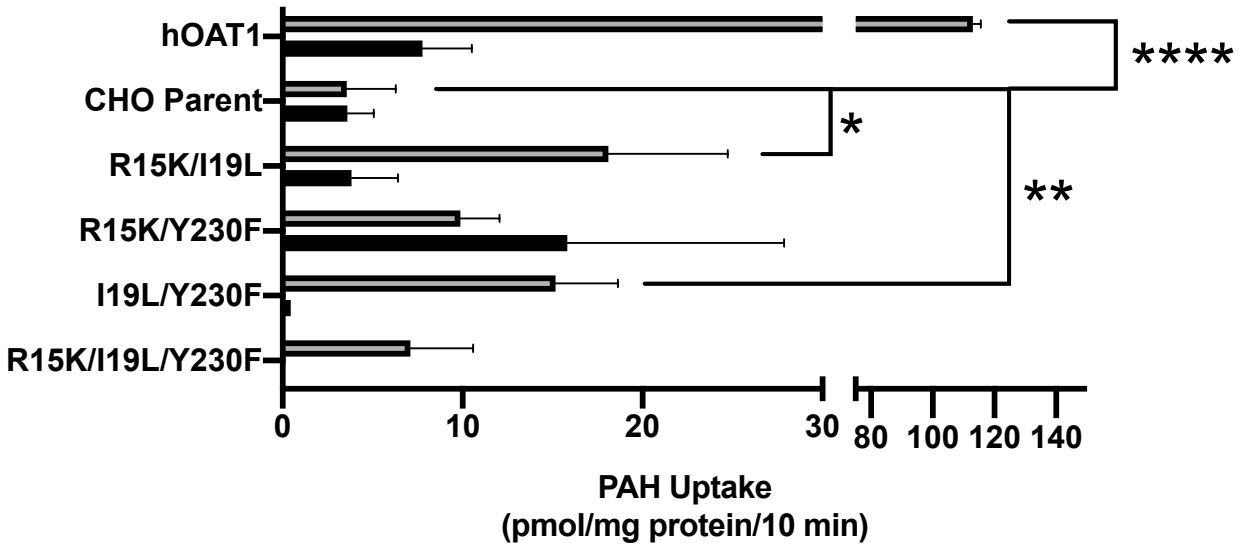

Figure 2.6. Round 1 functional screening of hOAT1 mutants.
Cells were incubated in 5 µM PAH spiked with 0.25 µCi/mL [H^3] PAH in the absence (gray) or presence (black) of 500 µM probenecid (inhibitor) for 10 min. Y-axis labels indicate the stably-expressing hOAT1 cell line tested including hOAT1 wild-type and the double and triple hOAT1 mutants. CHO parental cells were used as a measure of background activity. Accumulation values were normalized for protein content. Values reported as average ± SD of triplicate samples. Significance indicated by ****$p < 0.0001$, *$p < 0.05$ and **$p < 0.01$ compared to CHO parent as determined by one-way ANOVA followed by Dunnett's t-test. Image was generated using GraphPad Prism.

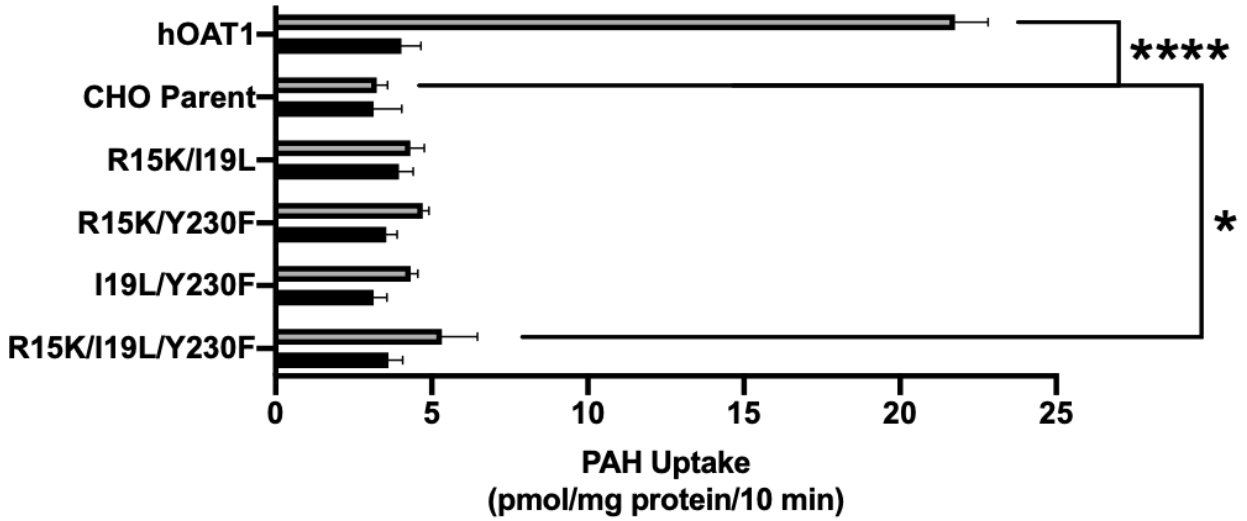

Figure 2.7. Round 2 functional screening of hOAT1 mutants.
Cells were incubated in 5μM PAH spiked with 0.25 μCi/mL [H^3] PAH in the absence (gray) or presence (black) of 500μM probenecid (inhibitor) for 10 min. Y-axis labels indicate the stably-expressing hOAT1 cell line tested including hOAT1 wild-type and the double and triple hOAT1 mutants. CHO parental cells were used as a measure of background activity. Accumulation values were normalized for protein content. Values reported as average ± SD of triplicate samples. Significance indicated by ****$p < 0.0001$ and *$p < 0.05$ compared to CHO parent as determined by one-way ANOVA followed by Dunnett's t-test. Image was generated using GraphPad Prism.

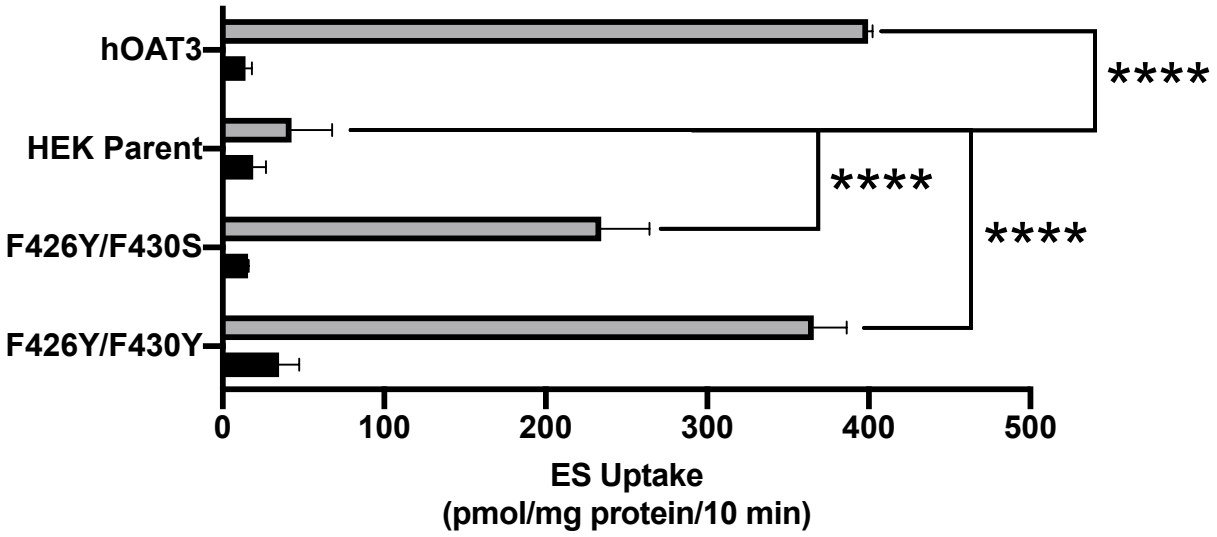

Figure 2.8. Representative functional screening of hOAT3 mutants.
Cells were incubated in 5 µM ES spiked with 0.25 µCi/mL [H^3] ES in the absence (gray) or presence (black) of 500 µM probenecid (inhibitor) for 10 min. Y-axis labels indicate the stably-expressing hOAT3 cell line tested including hOAT3 wild-type and the double hOAT3 mutants. HEK 293 parental cells were used as a measure of background activity. Accumulation values were normalized for protein content. Values reported as average ± SD of triplicate samples. Significance indicated by ****$p < 0.0001$ compared to HEK 293 parent as determined by one-way ANOVA followed by Dunnett's t-test. The functional screen was repeated a second time for N=2. Image was generated using GraphPad Prism.

2.C.3 Kinetic Assays

Based on the hOAT1 Round 1 functional screen (Figure 2.6), Arg15Lys/Ile19Leu and Ile19Leu/Tyr230Phe appeared to retain transport activity. Therefore, saturation analysis was conducted on these mutants to determine PAH affinity changes compared to hOAT1 wild-type. However, no transport activity was observed for any of the active hOAT1 mutants (data not shown). Subsequently, a time course experiment was conducted to determine if the linear range of uptake was extended for each mutant (Figure 2.9). As shown, substrate uptake in hOAT1 wild-type and hOAT1 mutants is linear through one min and 10 min, respectively. Therefore, a second kinetic assay (1-200 μM PAH) was conducted with an increased accumulation time of 10 min for each mutant was performed. No transport activity was observed for Ile19Leu/Tyr230Phe (data not shown) while potential transport activity was observed for Arg15Lys/Ile19Leu (Figure 2.10). It was unclear whether Arg15Lys/Ile19Leu was saturated with PAH at increasing concentrations of 1-200 μM. An additional assay was conducted with a broader PAH concentration range (10-2000 μM), however saturable Arg15Lys/Ile19Leu mediated uptake was not observed (Figure 2.11).

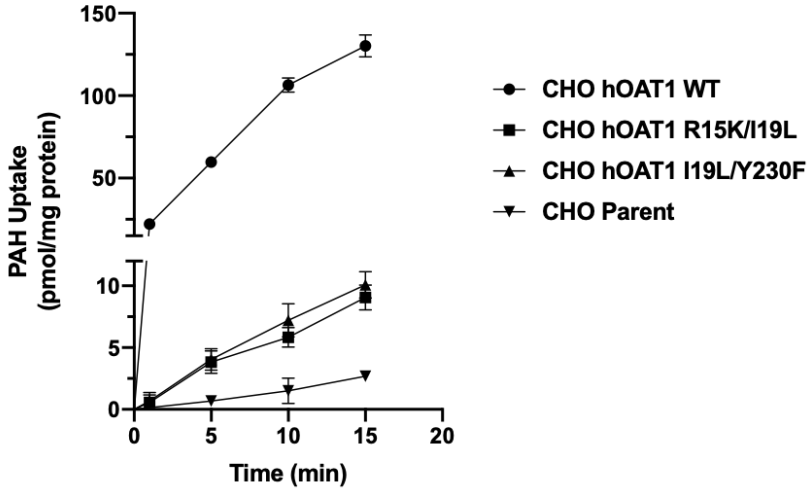

Figure 2.9. Representative time course of PAH uptake by hOAT1 wild-type and hOAT1 active mutants.
Cells were incubated in 5 μM PAH spiked with 0.25μCi/mL [H^3] PAH for 1–15 min. Accumulation values were corrected for background and protein content. Values reported as average ± SD of triplicate samples. The time course was repeated a second time for N=2. Image generated using GraphPad Prism.

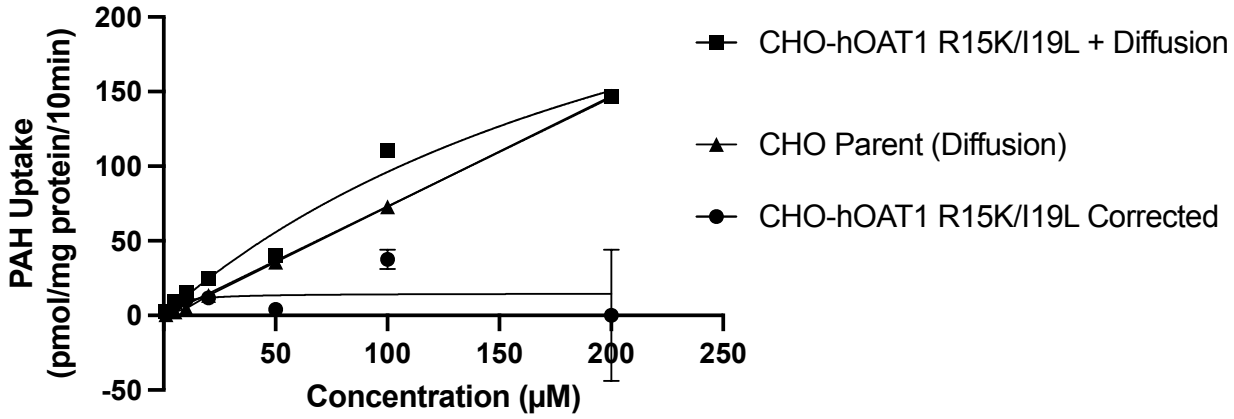

Figure 2.10. Saturation analysis of CHO hOAT1 Arg15Lys/Ile19Leu
CHO hOAT1 Arg15Lys/Ile19Leu was incubated in increasing concentrations of PAH (1–200 μM) spiked with 0.25μCi/mL [H^3] PAH for 10 min. Values were corrected for background and protein content. Image generated using GraphPad Prism.

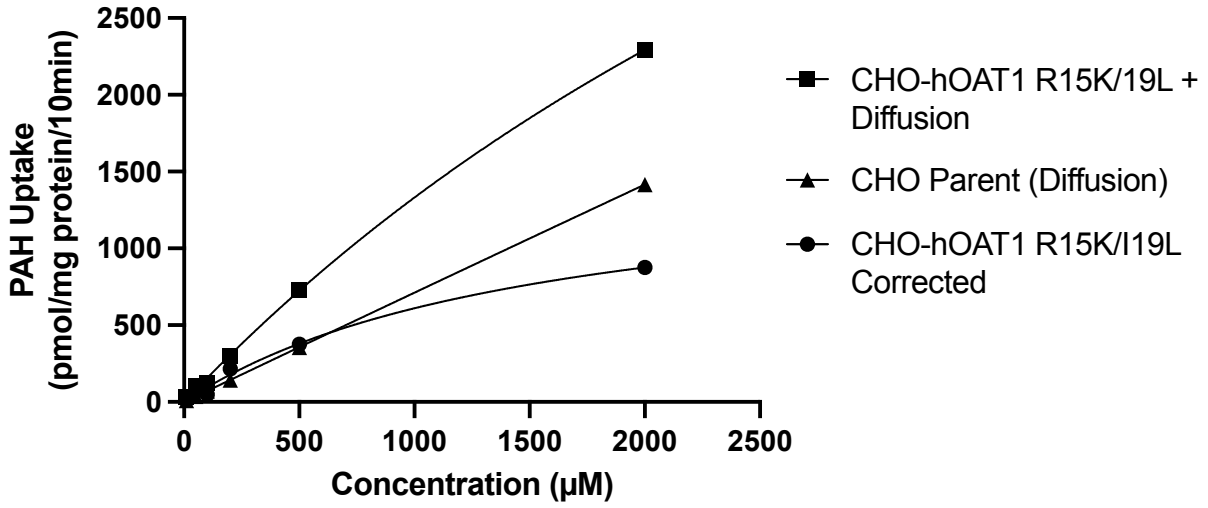

Figure 2.11. Saturation analysis of CHO hOAT1 Arg15Lys/Ile19Leu.
CHO hOAT1 Arg15Lys/Ile19Leu was incubated in increasing concentrations of PAH (10–2000 µM) spiked with 0.25µCi/mL [H^3] PAH for 10 min. Values were corrected for background and protein content. Image generated using GraphPad Prism.

Kinetic analysis was performed on transport active hOAT3 mutants to determine changes in K_m compared to hOAT3 wild-type. All mutant expressing cell lines showed saturable transport activity (Figure 2.12) and final K_m estimates are summarized in Table 2.5. As shown, neither hOAT3 mutant Phe426Tyr/Phe430Ser (14.4 ± 3.0 pmol/mg protein/1 min) nor Phe426Tyr/Phe430Tyr (16.7 ± 0.3 pmol/mg protein/1 min) exhibited statistically different K_m estimates as compared to wild-type hOAT3 (12.5 ± 3.4 pmol/mg protein/1 min).

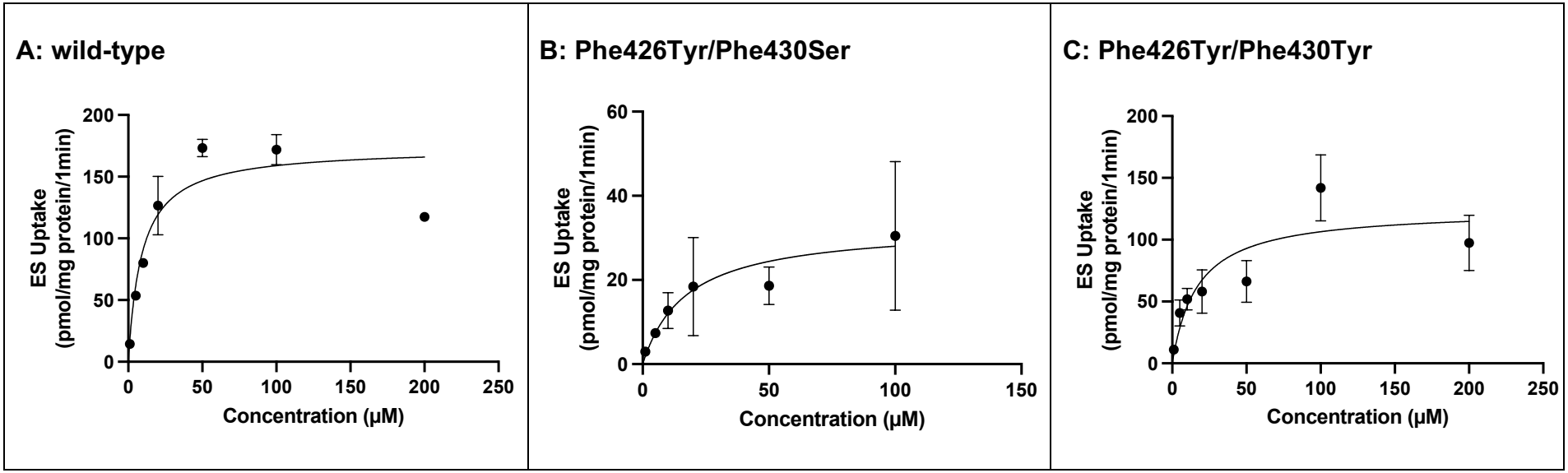

Figure 2.12. Representative saturation analysis for hOAT3 wild-type and active mutants.
(A) hOAT3 wild-type, **(B)** hOAT3 Phe426Tyr/Phe430Ser, and **(C)** hOAT3 Phe426Tyr/Phe430Tyr cell lines were incubated in increasing concentrations of ES (1–200 μM) spiked with 0.25μCi/mL [H^3] ES for 1 min. Values were corrected for background and protein content. K_m estimates were determined using Michaelis-Menten nonlinear regression in GraphPad Prism and reported as average ± SD of triplicate samples. A representative curve of the cell lines is shown in each panel. For hOAT3 wild-type and Phe426Tyr/Phe430Ser, saturation assays were repeated three times for N=3. For hOAT3 Phe426Tyr/Phe430Tyr, saturation assays were repeated twice for N=2.

Table 2.5. Estimated K_m for hOAT3 wild-type and hOAT3 active mutants.

Transporter	K_m (μM)	N
hOAT3 wild-type	12.5 ± 3.4	3
hOAT3 F426Y/F430S	14.0 ± 1.8	3
hOAT3 F426Y/F430Y	16.7 ± 0.3	2

Values reported as average ± SE.

2.D DISCUSSION

There has been increasing interest in OATs as they are known to interact with a broad variety of structurally diverse substrates, which makes them key contributors to the pharmacokinetics of many therapeutics as well as highly susceptible to drug-drug interactions. Therefore, from a clinical standpoint, gaining a better understanding of the biochemical interactions between hOATs and their substrates is essential to improve drug efficacy, better manage and predict drug-drug interactions, and even potentially influence drug design. Currently, there is no solved crystal structure for any of the OATs, and because of this lack of structural information, it is difficult to study OAT-substrate binding interactions. For this reason, *in silico* homology models of hOAT1 and hOAT3 were previously generated using the solved crystal structure of PiPT as template [8]. PiPT is currently the best available template as it belongs to the same transporter superfamily, shares relatively high protein sequence similarity to hOAT1 (33%) and hOAT3 (31%), is evolutionarily related to the OATs, as it is a eukaryotic protein, and is crystalized in its occluded state [8]. In addition, the International Transporter Consortium (ITC) has identified PiPT as the preferred template moving forward [19]. Previously, docking studies were performed between the hOAT1 and hOAT3 homology models and their prototypical substrates to determine amino acid residues that may potentially be involved in substrate recognition [8]. Single mutants were generated at the predicted contact amino acids, screened for transport activity, and kinetic analysis was pursued with transport active mutants. Findings from this previous study indicated that a single mutation is insufficient to elicit a statistically significant change in binding affinity of prototypical substrates [8].

Therefore, in this project, we study the impact of double and triple mutant combinations on binding affinity.

In order to test whether the previously generated hOAT1 and hOAT3 single mutants would bring about a significant change in affinity when combined, double and triple mutants were generated for hOAT1 and hOAT3 as appropriate (Table 2.1 and Table 2.2). For hOAT1, the Round 1 functional screen (Figure 2.6) revealed what appeared to be two active mutants (Arg15Lys/Ile19Leu, $p < 0.05$ and Ile19Leu/Tyr230Phe, $p < 0.01$). Not only was their PAH accumulation statistically significantly different from CHO parent, it was also at least two to three times above CHO parental background which is the standard criteria for determining whether a system is sufficiently robust to pursue kinetic analysis. However, a saturation assay at 1-200 μM PAH and one minute uptake showed no saturable transport activity (data not shown). To explore the possibility that the hOAT1 mutants had an extended linear range of uptake and that an extended accumulation time was required for sufficient signal to accumulate, a time course experiment was conducted. It was determined that the linear range of uptake was extended through at least 10 min for both hOAT1 active mutants (Figure 2.9). Upon conducting saturation experiments for 10 min, no transport activity was observed for Ile19Leu/Tyr230Phe, but no transport activity (K_m = 5.1 ± 12 μM) was detected for Arg15Lys/Ile19Leu (Figure 2.10). The hOAT1 Arg15Lys/Ile19Leu mutation may have resulted in a weaker binding affinity (increased K_m), so the PAH concentration range for the saturation assay was extended in order to ensure accurate K_m estimation. Therefore, another saturation assay from 10-2000 μM PAH with 10 min uptake was conducted. However, robust, saturable transport activity for hOAT1 Arg15Lys/Ile19Leu (K_m = 1542.2 ± 1379.2 μM) was not observed under these

conditions (Figure 2.11). Given the lack of uptake and extreme error associated with attempted kinetic analysis, the mutant appeared transport inactive. Therefore, the single functional screen (Figure 2.6) was repeated as statistically different transport activity seen in the Round 1 functional screen may have been due to improper washing following substrate exposure. In the Round 2 functional screen (Figure 2.7), where washing volume and time were increased post-substrate incubation to minimize variation between replicates, all hOAT1 mutants were found to be inactive, as PAH accumulation was not significantly different from CHO parental background. While Arg15Lys/Ile19Leu/Tyr230Phe was statistically significant compared to hOAT1 wild-type, the PAH accumulation was not two to three times CHO parental background activity, a required parameter in order to have a system that is considered robust enough to pursue kinetic analyses. Additionally, a paired t-test comparing PAH in the presence and absence of probenecid for Arg19Lys/Ile19Leu/Tyr230Phe indicated that there is no statistical difference ($p < 0.05$) between the two, suggesting once again that the triple mutant is transport inactive. The single mutations Arg15Lys, Ile19Leu, and Tyr230Phe were considered transport active mutants in previous studies [8]. Double and triple combinations of these hOAT1 mutants resulted in transport inactivity, potentially indicating that these mutations have disrupted multiple contacts within the binding site and that multiple substrate contacts are needed to stably bind and translocate PAH. These findings suggest that the hydrogen bond (Arg15), hydrophobic interaction (Ile19), and edge-face Pi system (Tyr230) all need to be present in order for the transporter to recognize PAH [8]. Since all hOAT1 mutants were considered transport inactive as there

was insufficient transport activity to pursue kinetic analysis, no further studies were conducted.

PAH transport inactivity observed for the hOAT1 mutants may be due to the following: 1) the mutation disrupted binding interaction(s) critical for substrate recognition or 2) the mutation disrupted proper protein folding and/or targeting to the plasma membrane. Previously, hOAT1 membrane localization via Western blotting, GFP-fusion constructs, and c-Myc tagged constructs was attempted, however all with inconclusive results [8]. When examined in hOAT1, hOAT2 and hOAT3 expressing cell lines, no transporter specific signal was associated with the commercial hOAT1 or hOAT3 antibodies via Western blotting [8]. The GFP-fusion constructs exhibited extensive cytoplasmic fluorescent signal, preventing conclusive evaluation at the cell surface (i.e., membrane targeting) [8]. Immunohistochemistry was conducted on c-Myc tagged constructs with a commercial c-Myc antibody, but again no transporter specific signal was observed for controls [8]. Membrane targeting of inactive mutant transporter constructs remains an unresolved issue.

Initial functional screening indicated both hOAT3 double mutants, Phe426Tyr/Phe430Ser and Phe426Tyr/Phe430Tyr ($p < 0.0001$), retained ES transport activity that is statistically different from HEK 293 parental background (Figure 2.8). Based on the functional screen, both hOAT3 mutants recognize and transport ES, but it is unknown whether the double mutant combinations altered the affinity for ES. Therefore, saturation assays were conducted on these mutants to estimate the kinetic parameter K_m (Figure 2.12). For the current study, the hOAT3 wild-type K_m for ES is 12.5 ± 3.4 μM (Table 2.5), which is in agreement with previous literature values [22]. In previous single

mutant studies, the estimated K_m values for Phe426Tyr (13.4 ± 2.9 μM) and Phe430Tyr (13.6 ± 0.2 μM) were not significantly different from wild-type [8]. However, the estimated K_m value for the combined Phe426Tyr/Phe430Tyr mutant (16.7 ± 0.3 μM) found in this study is similar to that of hOAT3 wild-type (Table 2.5). Similarly, the estimated K_m value for Phe426Tyr/Phe430Ser (14.4 ± 3.0 μM) is not significantly different from hOAT3 wild-type (Table 2.5). Previously, there was a significant increase in K_m with the single mutant Phe430Ser (26.8 ± 5.0 μM) [8]. Surprisingly, in combination with Phe426Tyr (Phe426Tyr/Phe430Ser) exhibited affinity similar to that of wild-type hOAT3. These findings suggest that Phe426 and Phe430 may somehow interact with each other in order to bind ES. Perhaps, the hydroxyl groups on the tyrosine and serine at both of these amino acid positions is necessary for the hydrophobic interactions that occur and having just one amino acid mutated disrupts the molecular interactions that occur.

In summary, initial accumulation assays demonstrated that double and triple combination mutations resulted in loss of transport activity in all hOAT1 mutants. There was no loss in transporter function for hOAT3 double combination mutations at positions 426 and 430. Furthermore, hOAT3 double mutants did not significantly alter the binding affinity, indicating a degree of tolerance as well as a potential interaction between the amino acids at these positions. Future work will focus on proper protein trafficking to the plasma membrane, which would strengthen the interpretation that these contact points actually play a role in substrate binding interactions. While all hOAT1 multiple mutants resulted in a complete loss of transport activity for PAH, these mutants could retain transport function for other substrates as they may have different amino acid contacts. Future work will evaluate the impact of these hOAT1 mutants on transport activity of other

hOAT1 substrates. Based on this study, it may be possible that hOAT3 positions 426 and 430 work in conjunction for ES recognition. In the future, kinetic studies with other hOAT3 substrates can further characterize these amino acid contacts. Once better characterized, hOAT1 and hOAT3 modeling studies could serve as tools to asses and optimize new chemical entities in terms of drug design. Furthermore, modeling studies could be utilized to predict drug-drug interactions, which aids in decisions for continued finance and pursuit of an investigational new drug.

LIST OF REFERENCES

1. **U.S. Food and Drug Administration**. In Vitro Drug Interaction Studies-Cytochrome P450 Enzyme-and Transporter-Mediated Drug Interactions Guidance for Industry. 2020.
2. **Agilent Technologies**. QuikChange Lightning Site-Directed Mutagenesis Kit. 2011.
3. **Bai X**, **Moraes TF**, **Reithmeier RAF**. Structural Biology of Solute Carrier (SLC) Membrane Transport Proteins. *Mol Membr Biol* 34: 1–32, 2017.
4. **Burckhardt G**. Drug Transport by Organic Anion Transporters (OATs). *Pharmacol. Ther.* 136: 106–130, 2012.
5. **Cihlar T**, **Lin DC**, **Pritchard JB**, **Fuller MD**, **Mendel DB**, **Sweet DH**. The Antiviral Nucleotide Analogs Cidofovir and Adefovir are Novel Substrates for Human and Rat Renal Organic Anion Transporter 1. *Mol Pharmacol* 56: 570–580, 1999.
6. **Ellison DH**. Clinical Pharmacology in Diuretic Use. *Clin J Am Soc Nephrol* 14: 1248–1257, 2019.
7. **Eraly SA**, **Vallon V**, **Vaughn DA**, **Gangoiti JA**, **Richter K**, **Nagle M**, **Monte JC**, **Rieg T**, **Truong DM**, **Long JM**, **Barshop BA**, **Kaler G**, **Nigam SK**. Decreased Renal Organic Anion Secretion and Plasma Accumulation of Endogenous Organic Anions in OAT1 Knock-Out Mice. *J Biol Chem* 281: 5072–5083, 2006.
8. **Jay C**. 3-D Homology Modeling of Organic Anion Transporters (OATS): Defining the Biochemical Basis for OAT-Substrate Interactions. 2019.
9. **Koepsell H**. The SLC22 Family With Transporters of Organic Cations, Anions and Zwitterions. *Mol Aspects Med* 34: 413–435, 2013.
10. **Invitrogen**. Lipofectamine 2000 User Guide. 2013.
11. **Lai RE**, **Jay CE**, **Sweet DH**. Organic Solute Carrier 22 (SLC22) Family: Potential for Interactions With Food, Herbal/Dietary Supplements, Endogenous Compounds, and Drugs. *J. Food Drug Anal.* 26: S45–S60, 2018.
12. **Lin L**, **Yee SW**, **Kim RB**, **Giacomini KM**. SLC Transporters as Therapeutic Targets: Emerging Opportunities. *Nat. Rev. Drug Discov.* 14: 543–560, 2015.
13. **European Medicines Agency**. Guideline on the Investigation of Drug Interactions. 2012.
14. **Mor AL**, **Kaminski TW**, **Karbowska M**, **Pawlak D**. New Insight Into Organic Anion Transporters From the Perspective of Potentially Important Interactions and Drugs Toxicity. *J. Physiol. Pharmacol.* 69: 307–324, 2018.
15. **Motohashi H**, **Saito H**, **Masuda S**, **Fukatsu A**. Gene Expression Levels and Immunolocalization of Organic Ion Transporters in the Human Kidney. *J Am Soc Nephrol* 13: 866–874, 2002.
16. **Nigam SK**, **Bush KT**, **Martovetsky G**, **Ahn S-Y**, **Liu HC**, **Richard E**, **Bhatnagar V**, **Wu W**. The Organic Anion Transporter (OAT) Family: A Systems Biology Perspective. *Physiol Rev* 95: 83–123, 2015.
17. **Perry JL**, **Dembla-Rajpal N**, **Hall LA**, **Pritchard JB**. A Three-Dimensional Model of Human Organic Anion Transporter 1: Aromatic Amino Acids Required for Substrate Transport. *J Biol Chem* 281: 38071–38079, 2006.
18. **Qiagen**. QIAprep Miniprep Handbook. 2020.
19. **Schlessinger A**, **Yee SW**, **Sali A**, **Giacomini KM**. SLC classification: An update.

Clin. Pharmacol. Ther. 94: 19–23, 2013.
20. **Sekine T**, **Endou H**. Immunolocalization of Multispecific Organic Anion Transporters, OAT1, OAT2, and OAT3, in Rat Kidney. *J Am Soc Nephrol* 13: 848–857, 2002.
21. **Tojo A**, **Sekine T**, **Nakajima N**, **Hosoyamada M**, **Kanai Y**, **Kimura K**, **Endou H**. Immunohistochemical Localization of Multispecific Renal Organic Anion Transporter 1 in Rat Kidney. *J Am Soc Nephrol* 10: 464–471, 1999.
22. **Wang L**, **Sweet DH**. Renal Organic Anion Transporters (SLC22 Family): Expression, Regulation, Roles in Toxicity, and Impact on Injury and Disease. *AAPS J.* 15: 53–69, 2013.
23. **Zhu C**, **Nigam KB**, **Date RC**, **Bush KT**, **Springer SA**, **Saier MH**, **Wu W**, **Nigam SK**. Evolutionary Analysis and Classification of OATs, OCTs, OCTNs, and Other SLC22 Transporters: Structure-Function Implications and Analysis of Sequence Motifs. *PLOS One* 10:1–20, 2015.
24. **BioParadigms**. SLC Tables. http://slc.bioparadigms.org. 2019.